Water-gas-shift reaction on metal nanoparticles and surfaces

Ping Liu and José A. Rodriguez

Citation: The Journal of Chemical Physics **126**, 164705 (2007); doi: 10.1063/1.2722747
View online: http://dx.doi.org/10.1063/1.2722747
View Table of Contents: http://scitation.aip.org/content/aip/journal/jcp/126/16?ver=pdfcov
Published by the AIP Publishing

Water-gas-shift reaction on metal nanoparticles and surfaces

Ping Liu[a] and José A. Rodriguez
Department of Chemistry, Brookhaven National Laboratory, Building 555, Upton, New York 11973

(Received 5 January 2007; accepted 13 March 2007; published online 24 April 2007)

Density functional theory was employed to investigate the water-gas-shift reaction (WGS, $CO+H_2O \rightarrow H_2+CO_2$) on Au_{29} and Cu_{29} nanoparticles seen with scanning tunneling microscopy in model $Au/CeO_2(111)$ and $Cu/CeO_2(111)$ catalysts. Au(100) and Cu(100) surfaces were also included for comparison. According to the calculations of the authors, the WGS on these systems operate via either redox or associative carboxyl mechanism, while the rate-limiting step is the same, water dissociation. The WGS activity decreases in a sequence: $Cu_{29} > Cu(100) > Au_{29} > Au(100)$, which agrees well with the experimental observations. Both nanoparticles are more active than their parent bulk surfaces. The nanoscale promotion on the WGS activity is associated with the low-coordinated corner and the edge sites as well as the fluxionality of the particles, which makes the nanoparticles more active than the flat surfaces for breaking the O–H bond. In addition, the role of the oxide support during the WGS was addressed by comparing the activity seen in the calculations of the authors for the Au_{29} and Cu_{29} nanoparticles and activity reported for $X/CeO_2(111)$ and $X/ZnO(000\bar{1})$(X=Cu or Au) surfaces. © *2007 American Institute of Physics*. [DOI: 10.1063/1.2722747]

I. INTRODUCTION

The water-gas-shift (WGS) reaction ($CO+H_2O \rightarrow CO_2+H_2$) has attracted considerable interest, due to its application in the production of hydrogen for fuel cells. Recent experiments show that the Au or Cu nanoparticles supported on the oxides, such as ceria and titania, display higher activity in the WGS than the bulk materials and Cu-based catalysts used in the industry.[1–4] Indeed, extensive studies have been carried out to investigate the WGS on both bulk surfaces and the supported nanoparticles experimentally and theoretically. Reports in the literature, however, vary widely, and the nature of the active species remains elusive.[1,2,5–9] One of the controversies is the reaction mechanism. To date, two main reaction mechanisms have been proposed. One is a redox mechanism,[4,10–14] where CO reacts with an oxygen atom coming from water dissociation or the oxide support to form CO_2. The other is an associative mechanism,[15–17] where the main reaction intermediates are species such as formate, carbonate, or carboxyl, produced by the reaction of CO with terminal hydroxyl groups present in the surface of the catalyst. In addition, various effects have been proposed to be of fundamental importance to the catalytic activity of the supported nanoparticles, including size, shape, the metal oxidation state, the nature and the degree of reduction of the oxide support, and the metal-oxide interactions. There is a clear need for a better understanding of the underlying mechanism of the WGS over metal and metal/oxide catalysts for optimizing their performance.

To clarify several of these issues, in this article we employ density functional theory (DFT) to investigate the WGS on Au_{29} and Cu_{29} nanoparticles with a diameter of 1.2 nm seen with scanning tunneling microscopy in model $Au/CeO_2(111)$ and $Cu/CeO_2(111)$ catalysts.[5,18,19] These systems (see Fig. 1) expose a combination of (100) and (111) faces in a pyramidal structure. In a previous work,[20] we found that Au_{29} is able to dissociate H_2 spontaneously while the molecule interacts weakly with Au(100) or Au(111). Several factors contribute to the enhanced chemical activity of a Au_{29} particle: low-coordinated Au atoms, fluxionality, and ensemble effects.[20] In this study, Au(100) and Cu(100) surfaces are also included for comparison. The article is organized as follows. First, we will describe the details of our DFT calculations (Sec. II) and a microkinetic model used to calculate the WGS rate via different mechanisms (Sec. III). Second, the potential energy profiles for the WGS on the surfaces (Sec. IV A) and nanoparticles (Sec. IV B) are established using the results from the DFT calculations. In addition, the reaction mechanism and possible intermediates for each system are identified. With this basis, the overall rate of the WGS is estimated by using the microkinetic model and compared to experimental results reported in the literature (Sec. IV C).

II. THEORETICAL SECTION

In the present study, the unrestricted DFT calculations were performed using the DMOL^3 code, which allows the

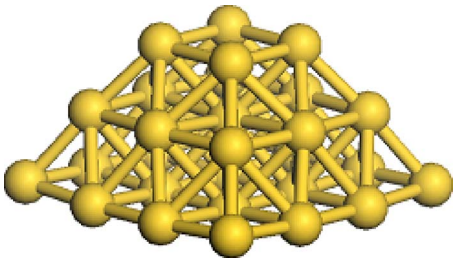

FIG. 1. (Color online) Structure for a Cu_{29} and a Au_{29} nanoparticle seen on $CeO_2(111)$ with scanning tunneling microscopy (Ref. 19).

[a]Electronic mail: pingliu3@bnl.gov

study of molecular systems and periodic surfaces.[21] The ionic cores were described by effective core potentials. A numerical basis set was used with comparable accuracy to a Gaussian 6-31G(d) basis set.[21] Since the numerical basis set used here is of a very high quality,[21] the basis set superposition error is minimized and should be comparable for molecules and solids, which is on the order of $<10\%$ of the reported energies.[21–23] A local basis cutoff of 5.0 Å in real space was employed. This basis set and cutoff were used in previous studies dealing with Au nanoparticles and gave a very good description of their properties.[18,20] The generalized gradient approximation (GGA) with the PW91 functional[24] was utilized in the present work. Our main interest here is the trends in the energetics, and in test calculations they were not affected when other GGA functionals (RPBE, PB, and BLYP) were used.[20] Previous extensive studies have shown that DFT with GGA can precisely predict adsorption differences in a series of systems,[12,15,25] which is the objective in the present work.

To model the bulk surfaces, we followed the supercell approach with four-layer slabs and a 11 Å vacuum between the slabs. Enough K points (25) were selected for the surfaces. The adsorbate coverage was $\frac{1}{4}$ of a monolayer. At this coverage, there should not be significant adsorbate↔adsorbate repulsive interactions (i.e., the adsorption energies on bulk surfaces and nanoparticles can be compared), and the size of the unit cell does not lead to an unreasonable amount of computer time. The top two layers of the surfaces and the nanoparticles were allowed to fully relax with the adsorbates. Transition states here were identified using a combination of synchronous transit methods[26] and eigenvector following and verified by the presence of a single imaginary frequency from a sequential vibrational frequency analysis. Synchronous transit methods interpolate a reaction pathway to find a transition state, which was refined using eigenvector following.

III. MICROKINETICS

There have been two pathways proposed regarding the mechanism for the WGS: a regenerative redox mechanism and an associative mechanism.[27] In the redox mechanism, successive oxidation and reduction of the surface occurs as follows:

$$\mathrm{CO} + * \leftrightarrow * \mathrm{CO}, \tag{1}$$

$$\mathrm{H_2O} + * \leftrightarrow \mathrm{H_2O} *, \tag{2}$$

$$\mathrm{H_2O} * + * \leftrightarrow \mathrm{HO} * + \mathrm{H} *, \tag{3}$$

$$2\mathrm{HO} * \leftrightarrow \mathrm{H_2O} * + \mathrm{O} *, \tag{4a}$$

$$\mathrm{HO} * + * \leftrightarrow \mathrm{H} * + \mathrm{O} *, \tag{4b}$$

$$\mathrm{CO} * + * \mathrm{O} \leftrightarrow \mathrm{CO_2} + 2 *, \tag{5}$$

$$2\mathrm{H} * \leftrightarrow \mathrm{H_2} + 2 *. \tag{6}$$

Here "*" represents a surface site, and therefore "X*" stands for the adsorbate bonded to this site. Water dissociates into adsorbed oxygen (Fig. 2) and hydrogen atoms, and the adsorbed oxygen is then titrated by CO. The associative mechanism involves reaction through an adsorbed intermediate species such as formate, carbonate, or carboxyl (Fig. 2). For instance, the dissociated OH reacts with CO to form HCOO** (formate),

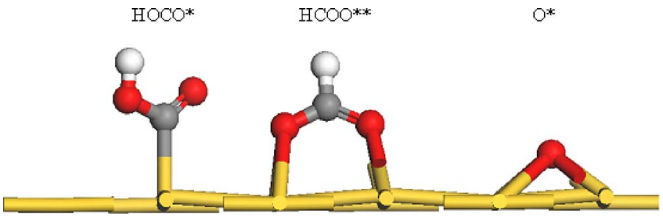

FIG. 2. (Color online) Schematics of some of the intermediates involved in the WGS (White: hydrogen; red or black: oxygen; and gray: carbon).

$$\mathrm{HO} * + \mathrm{CO} * \leftrightarrow \mathrm{HOOC}**, \tag{7a}$$

or OCOH * (carboxyl),

$$\mathrm{HO} * + \mathrm{CO} * \leftrightarrow \mathrm{OCOH} * + *, \tag{7b}$$

which eventually dissociates completely,

$$\mathrm{HCOO}** \leftrightarrow \mathrm{H} * + \mathrm{CO_2} + *, \tag{8a}$$

$$\mathrm{OCOH} * \leftrightarrow \mathrm{H} * + \mathrm{CO_2}, \tag{8b}$$

or decomposes in combination with OH,

$$\mathrm{HCOO}** + * \mathrm{OH} \leftrightarrow \mathrm{H_2O} * + \mathrm{CO_2} + 2 *, \tag{8c}$$

$$\mathrm{OCOH} * + * \mathrm{OH} \leftrightarrow \mathrm{H_2O} * + \mathrm{CO_2} + *, \tag{8d}$$

to form CO_2, H_2, and water. Here, the carbonate intermediate is not included in this study, as it is usually observed when oxides are involved.

On the basis of the calculated potential energy, we also take a further step to estimate the rate of the overall reaction (r) on each system. The slowest step among Eqs. (3), (4), (7), (8), and (5) was considered as the rate-limiting step (rls) in the present microkinetic model. All the other elementary steps were assumed in equilibrium, affecting only the number of free sites available for the rls. For the redox mechanism, the details of the rate calculations were shown in our previous work.[28] For the associative carboxyl mechanism, a dominant pathway as we will show in the next section, we write the site balance in terms of the adsorbed coverages of H_2O, H, CO, OH, OCOH, and free sites (*) as

$$\theta_{\mathrm{CO}} + \theta_{\mathrm{H_2O}} + \theta_{\mathrm{OH}} + \theta_{\mathrm{OCOH}} + \theta_{\mathrm{H}} + \theta_{*} = 1. \tag{9}$$

In the case that water dissociation [Eq. (3)] is the rls, the overall rate is expressed as

$$r = k_0 \exp\left(-\frac{\Delta E_{a(3)}}{k_B T}\right) P_{\mathrm{H_2O}} K_{(2)} \theta_*^2 \left(1 - \frac{P_{\mathrm{H_2}} P_{\mathrm{CO_2}}}{K_{\mathrm{gas}} P_{\mathrm{H_2O}} P_{\mathrm{CO}}}\right). \tag{10}$$

Here,

$$\theta_* = \frac{1}{1 + P_{CO}K_{(1)} + P_{H_2O}K_{(2)} + (P_{CO_2}/P_{CO}K_{(1)}K_{(7b)}K_{(8b)})\sqrt{P_{H_2}/K_{(6)}} + (P_{CO_2}/K_{(8b)})\sqrt{P_{H_2}/K_{(6)}} + \sqrt{P_{H_2}/K_{(6)}}}, \tag{11}$$

when the complete dissociation of carboxyl is preferred [Eq. (8b)], or

$$\theta_* = \frac{1}{1 + P_{CO}K_{(1)} + P_{H_2O}K_{(2)} + \sqrt{P_{CO_2}P_{H_2O}K_{(2)}/P_{CO}K_{(1)}K_{(7b)}K_{(8d)}} + \sqrt{P_{CO_2}P_{H_2O}P_{CO}K_{(1)}K_{(2)}K_{(7b)}/K_{(8d)}} + \sqrt{P_{H_2}/K_{(6)}}}, \tag{12}$$

in the case of combined decomposition [Eq. (8d)]. k_0 is the prefactor and $P_{H_2}P_{CO_2}/K_{gas}P_{H_2O}P_{CO}$ measures the approach to equilibrium for the overall gas phase reaction, where K_{gas} is the corresponding equilibrium constant. $\Delta E_{a(n)}$ stands for the activation barrier of the rls (n). $K_{(n)}$ represents the equilibrium constant of step (n) in the WGS kinetics, and P_X is the partial pressure of gas-phase species X. $K_{(n)}$ is given by

$$K_{(n)} = \exp[-(\Delta E_{ads}^{(n)} - T\Delta S_{(n)})/k_BT], \tag{13}$$

where $\Delta E_{ads}^{(n)}$ and $\Delta S_{(n)}$ are the changes in the enthalpy and entropy of the reactions, respectively. $\Delta E_{ads}^{(n)}$ is obtained from our DFT calculations.

If the formation of carboxyl is the rls [Eq. (7b)],

$$r = k_0 \exp\left(-\frac{\Delta E_{a(7b)}}{k_BT}\right)\frac{P_{CO}P_{H_2O}K_{(1)}K_{(2)}K_{(3)}\sqrt{K_{(6)}}}{\sqrt{P_{H_2}}} \times \theta_*^2\left(1 - \frac{P_{H_2}P_{CO_2}}{K_{gas}P_{H_2O}P_{CO}}\right), \tag{14}$$

with

$$\theta_* = \frac{1}{1 + P_{CO}K_{(1)} + P_{H_2O}K_{(2)} + P_{H_2O}K_{(2)}K_{(3)}\sqrt{K_{(6)}}/\sqrt{P_{H_2}} + (P_{CO_2}/K_{(8b)})\sqrt{(P_{H_2}/K_{(6)})} + \sqrt{(P_{H_2}/K_{(6)})}} \tag{15}$$

or

$$\theta_* = \frac{1}{1 + P_{CO}K_{(1)} + P_{H_2O}K_{(2)} + P_{H_2O}K_{(2)}K_{(3)}\sqrt{K_{(6)}}/\sqrt{P_{H_2}} + P_{CO_2}\sqrt{P_{H_2}}/K_{(3)}\sqrt{K_{(6)}}K_{(8d)} + \sqrt{P_{H_2}/K_{(6)}}}. \tag{16}$$

When the complete dissociation of $OCOH^*$ [Eq. (8b)] is the rls,

$$r = k_0 \exp\left(-\frac{\Delta E_{a(8b)}}{k_BT}\right)\frac{P_{CO}P_{H_2O}K_{(1)}K_{(2)}K_{(3)}\sqrt{K_{(6)}}K_{(7b)}}{\sqrt{P_{H_2}}} \times \theta_*\left(1 - \frac{P_{H_2}P_{CO_2}}{K_gP_{H_2O}P_{CO}}\right), \tag{17}$$

and in the case of the combined decomposition of $OCOH^*$ with $^*OH$ as the rls,

$$r = k_0 \exp\left(-\frac{\Delta E_{a(8d)}}{k_BT}\right)\frac{P_{CO}P_{H_2O}^2K_{(1)}K_{(2)}^2K_{(3)}^2K_{(6)}K_{(7b)}}{P_{H_2}} \times \theta_*^2\left(1 - \frac{P_{H_2}P_{CO_2}}{K_gP_{H_2O}P_{CO}}\right), \tag{18}$$

where

$$\theta_* = \frac{1}{1 + P_{CO}K_{(1)} + P_{H_2O}K_{(2)} + P_{H_2O}K_{(2)}K_{(3)}\sqrt{K_{(6)}}/\sqrt{P_{H_2}} + P_{CO}P_{H_2O}K_{(1)}K_{(2)}K_{(3)}\sqrt{K_{(6)}}K_{(7b)}/\sqrt{P_{H_2}} + \sqrt{P_{H_2}/K_{(6)}}}. \tag{19}$$

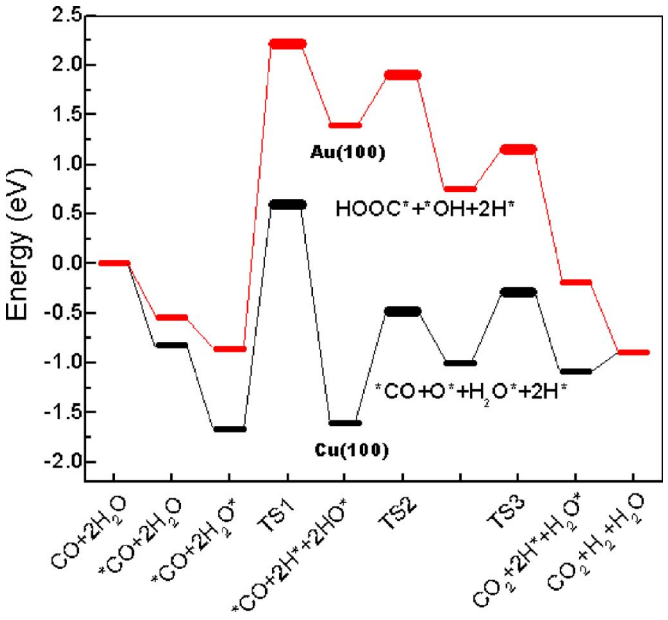

FIG. 3. (Color online) Potential energy diagram for the WGS on the Au(100) and Cu(100) surfaces. The zero energy is taken as the sum of the energies of the bare surface, gas-phase water, and carbon monoxide. "TS" represents the transition state.

Similar kinetic equations can be obtained when considering the associative format mechanism [Eq. (7a)]. However, we do not include these equations in the present paper because none of the systems under study adopts such a mechanism.

IV. RESULTS AND DISCUSSION

A. WGS on Au(100) and Cu(100) surfaces

The full energy profile for the WGS on Au(100) and Cu(100) surfaces including kinetic barrier is shown in Fig. 3. The energies are expressed with respect to the clean surface, a free CO molecule, and two H_2O molecules in the gas phase. As shown in Sec. III, the hydroxyl and the hydrocarbon intermediates undergo either the direct decomposition [Eqs. (4b), (8a), and (8b)] or dissociation in combination with OH [Eqs. (4a), (8c), and (8d)], where the latter requires at least two H_2O molecules to be involved. As will be seen below, this combined dissociation is preferred for the WGS reaction on both Au(100) and Cu(100). The adsorption configurations for the reactants, intermediates, and transition states (TS) involved in this process are displayed in Fig. 4.

On Au(100), CO adsorption [Eq. (1)] is exothermic and the bridging sites are preferred (Fig. 4) with a reaction energy of $\Delta E_{(1)}=-0.54$ eV (Fig. 3). H_2O molecules [Eq. (2)] are weakly adsorbed at the top sites with $\Delta E_{(2)}=-0.15$ eV (Fig. 3). This indicates that at typical catalytic conditions, e.g., 623 K, H_2O will not stick on the catalyst. The first and the most energy-consuming step is water dissociation [Eq. (3)] with a $\Delta E_{(3)}$ of +0.74 eV and a barrier ($\Delta Ea_{(3)}$) of +1.53 eV. As indicated before, there are several possibilities for the next step, where the reaction intermediates can be O^* [Eqs. (4a) and (4b)], $HCOO^{**}$ [Eq. (7a)], or $OCOH^*$ [Eq. (7b)]. We have carried out extensive TS calculations to find

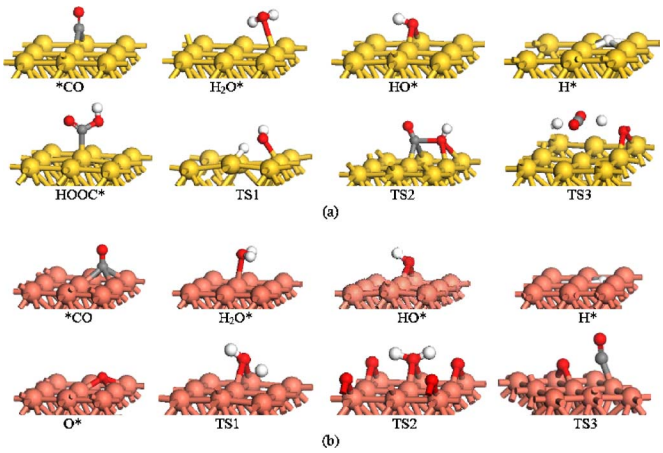

FIG. 4. (Color online) Structures of intermediates and transition states (TS) involved in the WGS on the surfaces of Au(100) (a) and Cu(100) (b). White: hydrogen; red or black: oxygen; gray: carbon; big yellow or light gray in part (a): gold; and big light red or dark gray in part (b): copper.

the energy barrier for each of these three reactions. The calculated barrier and the corresponding structure of the transition state are shown in Figs. 5 and 6, respectively. One can see that the WGS should follow the associative mechanism via carboxyl intermediates [Eq. (7b)], which gives a lower barrier ($\Delta E_{a_{(7b)}}=+0.51$ eV) than the other two processes ($\Delta E_{a_{(4b)}}=+0.73$ eV; $\Delta E_{a_{(7a)}}=+3.28$ eV). Interacting with $^*OH$ species, $OCOH^*$ dissociates to yield CO_2 gas and adsorbed H_2O [Eq. (8c)]. This is a highly exothermic step with the energy gain of −0.95 eV and a barrier of +0.40 eV. The last step, the desorption of H_2 [Eq. (6)], is also a downhill reaction ($\Delta E_{(6)}=-0.69$ eV). Overall, the WGS on Au(100) is via an associative carboxyl mechanism and water dissociation is the rls.

Cu(100) is much more reactive than Au(100). As shown in Fig. 4(b), CO adsorbs on fourfold hollow sites of Cu, and the binding energy is ~0.30 eV more stronger than that on Au(100) (Fig. 3). An increase in energy of 0.15 eV is also

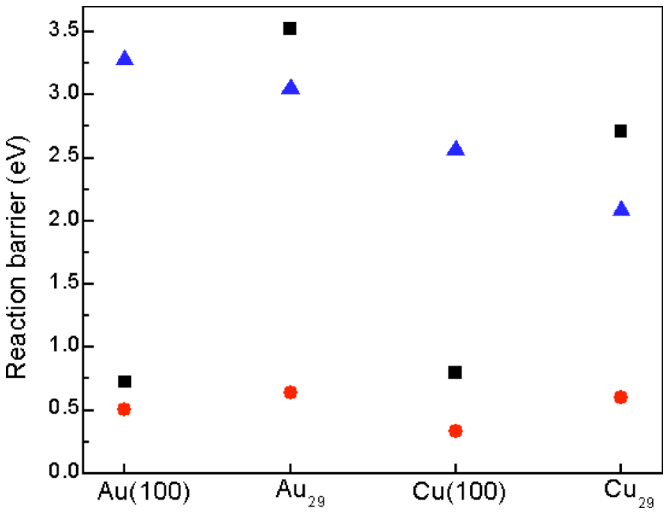

FIG. 5. (Color online) Calculated reaction barrier for the formation of $^*O$ ($2^*OH \rightarrow H_2O^* + {}^*O$ or $^*OH + * \rightarrow {}^*O + {}^*H$, ■ symbols), formation of carboxyl ($^*CO + {}^*OH \rightarrow OCOH^* + *$, ● symbols), and formation of format ($^*CO + {}^*OH \rightarrow HCOO^{**}$, ▲ symbols) on Au(100), Cu(100), Au_{29}, and Cu_{29}.

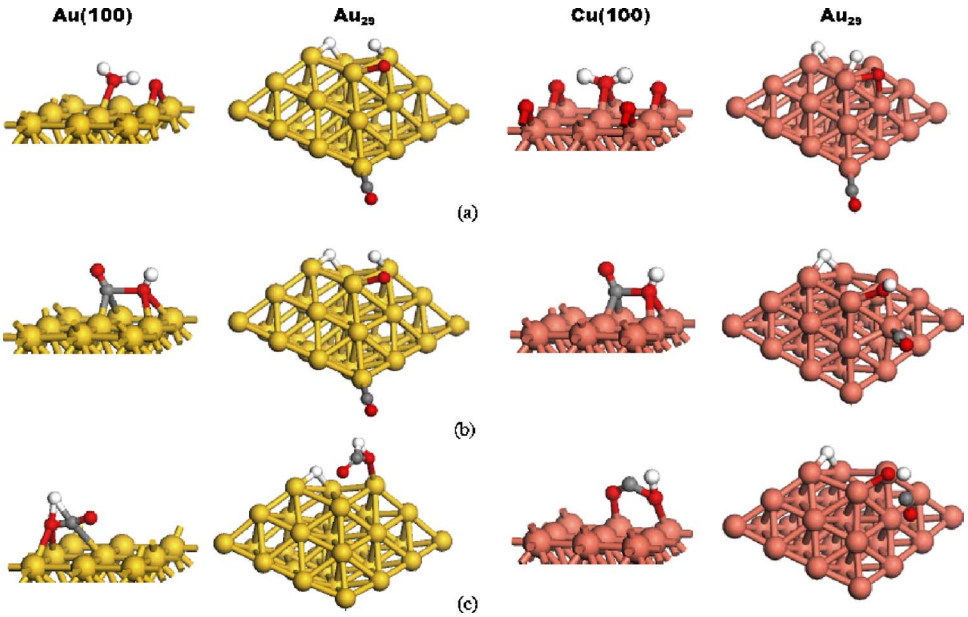

FIG. 6. (Color online) Structures of the transition states for the formation of $^*O$ (a), formation of carboxyl (b), and formation of format (c) on Au(100), Cu(100), Au_{29}, and Cu_{29}. White: hydrogen; red or black: oxygen; gray: carbon; big yellow or light gray: gold; and big light red or dark gray: copper.

observed for H_2O adsorbed on top of Cu (Fig. 4). The dissociation of a single H_2O on Cu(100) is less endothermic ($\Delta E_{(3)}=+0.39$ eV) and the corresponding barrier becomes lower ($\Delta E_{a_{(3)}}=+1.13$ eV). Similar results have also been reported recently for Cu(110), showing that the dissociation of a single H_2O is also difficult on this surface with a high barrier of 0.94 eV.[29] According to our calculations, the formation of format [Eq. (7a)] on Cu(100) should be also very unlikely ($\Delta E_{a_{(7a)}}=+2.56$ eV), and in contrast the dissociation of $^*OH$ [Eq. (4a)] and the formation of the carboxyl [Eq. (7b)] are much more facile with $\Delta E_{a_{(4b)}}=+0.80$ eV and $\Delta E_{a_{(7b)}}=+0.33$ eV (Fig. 5). It seems that the WGS should follow the associative carboxyl mechanism on Cu(100). However, our calculations show that different from the case of Au(100), the adsorbed carboxyl groups are not stable on Cu(100) and easily decomposes into OH^* and CO^*. Thus, reaction (4b) should be the operating step, and the produced $^*O$ eventually oxidizes $^*CO$ [Eq. (5)] ($\Delta E_{a_{(5)}}=+0.71$ eV). That is, in the case of Cu(100), the redox mechanism should be preferred and again water dissociation is the rls. On Cu(100) the $2H^* \rightarrow H_2$ reaction is slightly endothermic ($\Delta E_{(6)}=+0.2$ eV). T and P will particularly affect the chemical potential of gas-phase molecules. It is known that desorption processes, such as the $2H^* \rightarrow H_2$ reaction, are driven by a large entropy term at elevated temperatures, so the endothermic nature of the final step on Cu(100) or on the Au_{29} and Cu_{29} nanoparticles as we will see below, does not represent a significant problem. Compared to Au, Cu is more reactive, being able to bond the adsorbates more strongly, and consequently, the barrier for the dissociation reaction [Eq. (3)] is lowered. This trend agrees well with experimental results which indicate that Cu(100) or Cu(110) are good WGS catalysts while Au(111) or polycrystalline Au are very poor ones.[18,30]

B. WGS on Au_{29} and Cu_{29} nanoparticles

Figure 7 displays the energy profile for the WGS on Au_{29} and Cu_{29} nanoparticles, and the corresponding geometries of the intermediates and transition states are shown in Figure 8. Cu_{29} and Au_{29} exhibit a pyramidal structure formed by the interconnection of (111) and (100) faces of the bulk metals, see Fig. 1. These nanoparticles have been observed on $CeO_2(111)$ with scanning tunneling microscopy.[19] They had three layers (containing 16, 9, and 4 metal atoms) that expose different types of adsorption sites with a large degree of fluxionality.[20] Our calculations show that after full optimization, the geometries of Cu_{29} are distorted from a C_{4v} pyramid to a C_{2v} boat-shaped structure [Fig. 8(b)]. This distortion produces an arrangement of the atoms in the particle that gives a high number of atoms exposed in the (111) face, the most stable orientation for Cu. A similar distortion is also observed when the symmetry of Au_{29} is broken by interacting with the adsorbates [Fig. 8(a)], a phenomenon also observed in our previous study.[20] In addition, we checked that

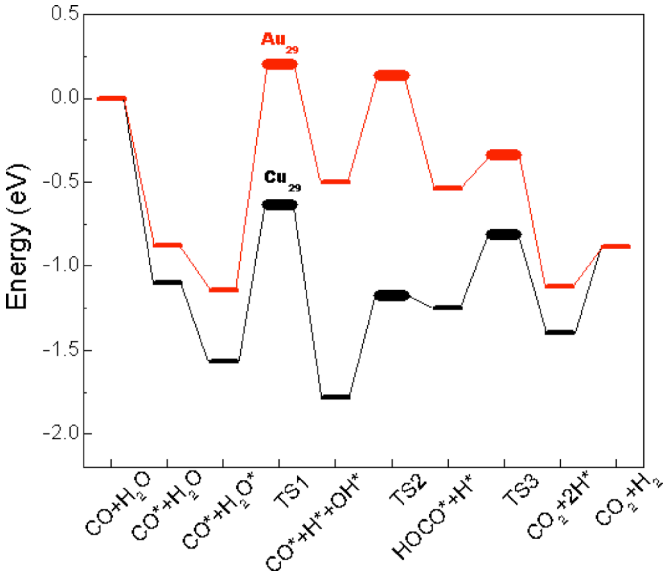

FIG. 7. (Color online) Potential energy diagram for the WGS on Au_{29} and Cu_{29} nanoparticles. The zero energy is taken as the sum of the energies of the bare nanoparticle, gas-phase water and carbon monoxide. "TS" represents the transition state.

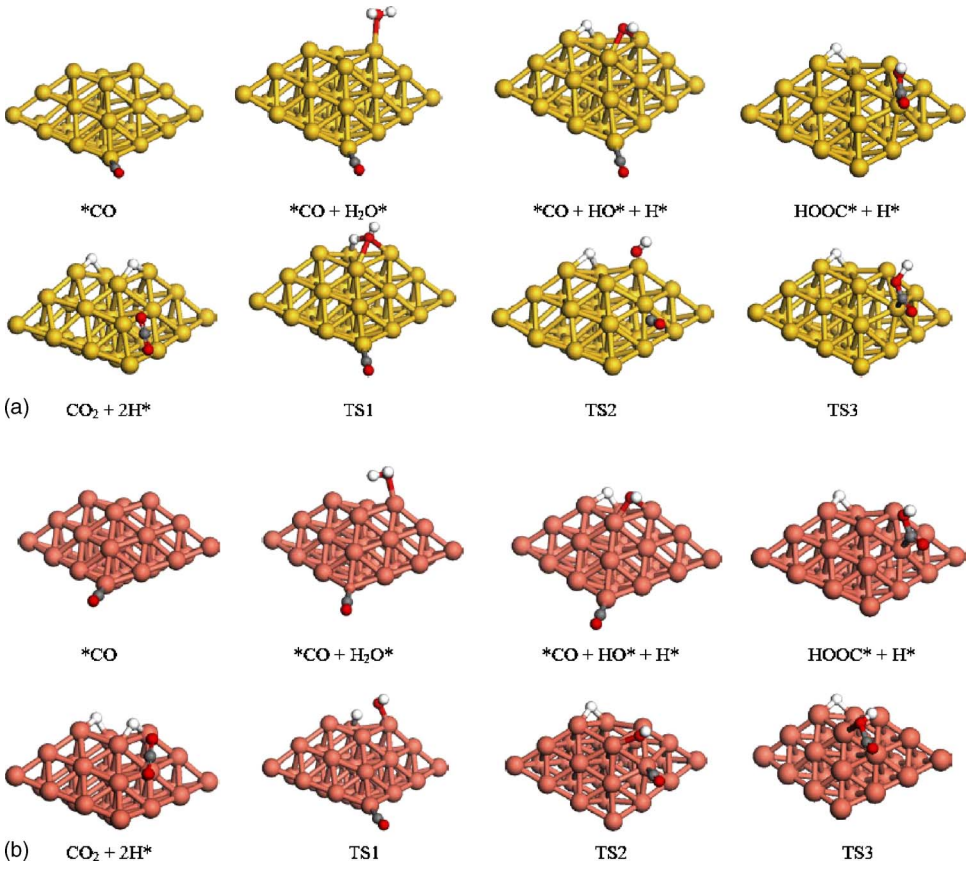

FIG. 8. (Color online) Structures of intermediates and transition states (TS) involved in the WGS on the surfaces of Au_{29} (a) and Cu_{29} (b). White: hydrogen; red or black: oxygen; gray: carbon; big yellow or light gray: gold; and big light red or dark gray: copper.

both distorted geometries do not have any imaginary frequency and therefore corresponds to local minima. Thus, Cu_{29} and Au_{29} can be taken as reasonable models for unsupported nanocatalysts. We note here that only one H_2O molecule is included for the WGS reaction on the nanoparticles. As indicated in the following, both Cu_{29} and Au_{29} can only dissociate one H_2O molecule at the top of the particles. Therefore, the second H_2O molecule can only be molecularly adsorbed and does not participate in the reaction since it easily desorbs at the WGS temperature.

According to our calculations, both nanoparticles are more active than their parent bulk materials during the reaction. Compared to Au(100), water and CO bond Au_{29} more strongly ($\Delta E_{(1)}=-0.88$ eV and $\Delta E_{(2)}=-0.27$ eV) by occupying the most favorable corner sites [Fig. 8(a)], which are generally considered more active than the terrace sites due to their low coordination.[22,31] When approaching water from the top of the nanoparticle, the lowest reaction barrier is found with both dissociated H and OH bridging one corner and one edge Au atom [Fig. 8(a)]. In fact, it has been reported that H_2 spontaneously dissociates at the same sites of Au_{29}, while just adsorbing on Au(100).[20] Similarly, upon moving from Au(100) to Au_{29}, our calculations show that $\Delta E_{(3)}$ and $\Delta E_{a_{(3)}}$ are lowered by 0.14 and 0.24 eV, respectively. Several factors contribute to the enhanced chemical activity of a Au particle: low-coordinated Au atoms, fluxionality, and ensemble effects. As in the case of Au(100), the WGS on Au_{29} is found to follow the associative carboxyl mechanism [Fig. 8(a)]. The formation of carboxyl is a thermoneutral reaction and gives a much lower barrier ($\Delta E_{a_{(7b)}}=+0.64$ eV) than the redox mechanism ($\Delta E_{a_{(4b)}}=+3.05$ eV) and the associative format mechanism ($\Delta E_{a_{(7a)}}=+3.51$ eV, Fig. 5). The dissociation of carboxyl [Eq. (8b)] is the only exothermic step during this process ($\Delta E_{(8b)}=-0.59$ eV) and the barrier is as low as 0.20 eV. Therefore, one can see that the WGS on Au_{29} follows the associative mechanism with water dissociation remaining as the rls. By using its corner and edge sites, Au_{29} exhibits higher activity than Au(100). Yet, it is not as active as Cu(100).

Cu_{29} is the most active among all the systems studied here, being able to strongly interact with the adsorbates (Fig. 7). Similar to the case of Au_{29}, both CO and water prefer to bond on top of corner sites. However, the corresponding binding energies are much stronger, with $\Delta E_{(1)}=-1.10$ eV and $\Delta E_{(2)}=-0.47$ eV [Figs. 7 and 8(b)], than on Au_{29} or Cu(100). The dissociation of water at the top of Cu_{29} [Fig. 8(b)] is exothermic ($\Delta E_{(3)}=-0.21$ eV), and the barrier is lowered to +0.93 eV. This indicates that the water dissociation on Cu_{29} is the most facile among all the systems investigated here. As shown in Fig. 5, the formation of carboxyl on Cu_{29} ($\Delta E_{a_{(7b)}}=0.60$ eV) is much more favorable than the formation of format ($\Delta E_{a_{(8a)}}=+2.08$ eV) and atomic oxygen ($\Delta E_{a_{(4b)}}=+2.71$ eV). That is, the WGS on Cu_{29} also adopts an associative mechanism via carboxyl, which dissociates into CO_2 and $^*H$ [Eq. (8b)] with an energy gain of –0.15 eV and a barrier of +0.44 eV. Therefore, the water dissociation should be the rls for the WGS on Cu_{29}.

Overall, the WGS follows different mechanisms over the

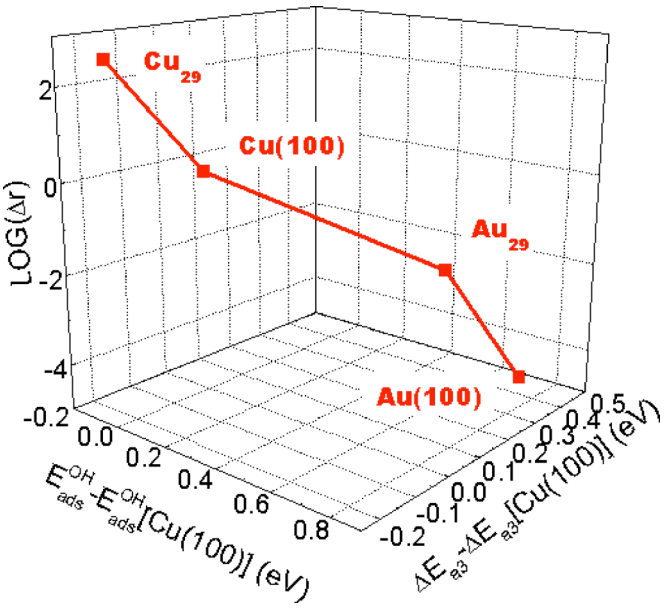

FIG. 9. (Color online) Correlation among the relative rate of the WGS (Δr), the relative hydroxyl adsorption energy, and the relative barrier for water dissociation on Cu(100), Au(100), Au_{29}, and Cu_{29} at typical WGS conditions (19 Torr of CO, 9 Torr of H_2O, 1 Torr of CO_2, and 1 Torr of H_2 at 625 K). Here the rate is expressed relative to the case of Cu(100) [Eq. (20)].

systems studied here, redox for Cu(100) and the associative carboxyl for Au(100), Au_{29}, and Cu_{29}. However, the rls is always the same: water dissociation.

C. Estimation of catalytic activity for the WGS reaction

On the basis of the microkinetic model of Sec. III and the DFT calculations, we take a further step to estimate the overall rate for the WGS under typical reaction conditions (19 Torr of CO, 9 Torr of H_2O, 1 Torr of CO_2, and 1 Torr of H_2 at 625 K). As we are interested in the change of the activity from one system to the next, the WGS reaction rate r here is expressed with respect to the case of Cu(100) as

$$\Delta r = \frac{r}{r^{\mathrm{Cu}(100)}}. \tag{20}$$

The results are shown in Fig. 9. Here, we take the adsorption energy of OH as an example to scale the bonding activity of the systems. In fact, a similar trend is observed when substituting CO or H for OH. It is shown that the bonding activity (x axes), the barrier for the rls (water dissociation, y axes), and the relative rates (z axes) for the WGS are strongly correlated. The higher the binding activity, the lower the barrier for the water dissociation and therefore the faster the WGS. One can thus see that the bonding energy to the intermediates is the essential factor that determines the speed of water dissociation and therefore the WGS reaction. Cu_{29} exhibits the highest rate towards the WGS, followed by Cu(100), then Au_{29}, and finally Au(100) in a decreasing sequence. It has been found that bulk Cu is the best metal catalyst for the WGS reaction by displaying a moderate bonding towards the reactants, intermediates, and products.[12] Our results also show that Au(100) is too inert to dissociate water and the reaction cannot proceed on this surface. In contrast, Cu(100) is more active and catalyzes the reaction in a reasonable rate, which is $\sim 10^5$ faster. A rate increase of $\sim 10^3$ is also observed when going from Au(100) to Au_{29}. A similar effect of size is observed for the case of Cu, where the WGS on Cu_{29} runs faster than on Cu(100) by a factor of $\sim 10^3$. The superior activity of the nanoparticles over their parent bulk surfaces is associated with the corner and the edge sites, which are more active than the terrace sites. In addition, one can also see in Fig. 8 that both nanoparticles are distorted when they interact with the adsorbates to stabilize the conformation, while on the flat surfaces, only small changes of the geometries are observed (Fig. 4). Therefore, the fluxionality of the particle also contributes, which makes the nanoparticles more adaptable towards the bindings of reactants and intermediates than the flat surfaces. Given that, the dissociation of water becomes more facile on the nanoparticles than on the corresponding bulk surfaces.

In fact, our calculations agree well with the results of experiments,[18] which show a decrease of the WGS reactivity according to the sequence: $Cu/ZnO(000\bar{1}) > Cu(100) > Au/ZnO(000\bar{1}) > Au(111)$. In the experimental studies,[18] ZnO was found to act only as a support for the nanoparticles and did not participate in the reaction, consistent with an earlier proposition by Campbell and co-workers.[30] In addition, both the experiment and the calculations find that the increase in the WGS activity by forming nanoparticles has its limits. As indicated above, the barrier for the water dissociation on the surfaces is only lowered by ~ 0.2 eV after forming nanoparticles. This, however, is not the case for a CeO_2 support, since a significant improvement has been observed when going from $Au/ZnO(000\bar{1})$ to $Au/CeO_2(111)$, although the Au nanoparticle size is about the same in both systems.[18] Is that due to the effect of ceria on the oxidation state of the supported particles? We have investigated the water dissociation on the nanoparticle ions ($Au_{29}^{\pm}$ and $Cu_{29}^{\pm}$).[18] The results show that charging both nanoparticles to form cations or anions does not help the O–H bond cleavage at all. Therefore, in this case, ceria must be directly involved in the WGS to lower the barrier of water dissociation and facilitate the reaction.

V. CONCLUSIONS

DFT-GGA calculations were employed to investigate the WGS on Cu and Au systems including both surfaces and nanoparticles. Our results show that the WGS follows a redox mechanism on Cu(100), while the associative mechanism via a carboxyl intermediate is preferred for Au(100), Au_{29}, and Cu_{29}. However, the rls step for all of these systems is the same: water dissociation.

In addition, WGS activity was found to decrease in a sequence: $Cu_{29} > Cu(100) > Au_{29} > Au(100)$. Au(100) is too inert to dissociate water. In contrast Cu(100) is more active, being able to catalyze the reaction with a reasonable rate. In addition, it was also shown that both nanoparticles are more active than their parent bulk surface. The enhanced WGS activity of the nanoparticles is associated with the low-coordinated corner and the edge sites, which are more active

than the sites present in flat surfaces, as well as the fluxionality of the particles, which contributes to the cluster stabilization. Given that, the dissociation of water becomes more facile when going from extended surfaces to nanoparticles. Nevertheless, these results cannot explain the high WGS activity observed for CeO_2-supported Au nanoparticles, where the support must be directly involved in the WGS to lower the barrier of water dissociation and facilitate the reaction.

ACKNOWLEDGMENTS

The research carried out at Brookhaven National Laboratory was supported by the U.S. Department of Energy, Division of Chemical Sciences, under Contract No. DE-AC02-98CH10886.

[1] Q. Fu, H. Saltsburg, and M. Flytzani-Stephanopoulos, Science **301**, 935 (2003); W. Deng and M. Flytzani-Stephanopoulos, Angew. Chem., Int. Ed. **45**, 2285 (2006).
[2] H. Sakurai, T. Akita, S. Tsubota, S. Kiuchi, and M. Haruta, Appl. Catal., A **291**, 179 (2005).
[3] H. Kusar, S. Hocevar, and J. Levec, Appl. Catal., B **63**, 194 (2006).
[4] Y. Li, Q. Fu, and M. Flytzani-Stephanopoulos, Appl. Catal., B **27**, 179 (2000).
[5] X. Wang, J. A. Rodriguez, J. C. Hanson, M. Perez, and J. Evans, J. Chem. Phys. **123**, 221101 (2005).
[6] Z. P. Liu, S. J. Jenkins, and D. A. King, Phys. Rev. Lett. **94**, 196102 (2005).
[7] D. Tibiletti, A. Amieiro-Fonseca, R. Burch, Y. Chen, J. M. Fisher, A. Goguet, C. Hardacre, P. Hu, and D. Thompsett, J. Phys. Chem. B **109**, 22553 (2005).
[8] X. Wang, J. A. Rodriguez, J. C. Hanson, D. Gamarra, A. Martinez-Arias, and M. Fernandez-Garcia, J. Phys. Chem. B **109**, 19595 (2005).
[9] V. Idakiew, T. Tabakova, A. Naydenov, Z. Y. Yuan, and B. L. Su, Appl. Catal., B **63**, 178 (2006).
[10] O. Jakdetchai and T. Nakajima, J. Mol. Struct.: THEOCHEM **619**, 51 (2002).
[11] C. Wheeler, A. Jhalani, E. J. Klein, S. Tummala, and L. D. Schmidt, J. Catal. **223**, 191 (2004).
[12] N. Schumacher, A. Boisen, S. Dahl, A. A. Gokhale, S. Kandoi, L. C. Grabow, J. A. Dumesic, M. Mavrikakis, and I. Chorkendorff, J. Catal. **229**, 265 (2005).
[13] C. V. Ovensen, B. S. Clausen, J. Schiøtz, P. Stoltze, H. Topsøe, and J. K. Nørskov, J. Catal. **168**, 133 (1997); C. V. Ovensen, P. Stoltze, J. K. Nørskov, and C. T. Campbell, *ibid.* **134**, 445 (1992).
[14] S. Hilaire, X. Wang, T. Luo, and R. J. Gorte, Appl. Catal., A **215**, 271 (2001).
[15] T. Shido and Y. Iwasawa, J. Catal. **141**, 71 (1993).
[16] G. Jacobs, L. Williams, U. Graham, D. Sparks, and B. H. Davis, J. Phys. Chem. B **107**, 10398 (2003).
[17] I. Fishtik and R. Datta, Surf. Sci. **512**, 229 (2002).
[18] J. A. Rodriguez, P. Liu, J. Hrbek, J. Evans, and M. Pérez, Angew. Chem., Int. Ed. **46**, 1329 (2007).
[19] S. Oyama, T. Ito, J. A. Rodriguez, and J. Nakamura (unpublished).
[20] L. Barrio, P. Liu, J. A. Rodríguez, J. M. Campos-Martín, and J. L. G. Fierro, J. Chem. Phys. **125**, 164715 (2006).
[21] B. Delley, J. Chem. Phys. **92**, 508 (1990); **113**, 7756 (2000).
[22] J. P. Perdew and Y. Wang, Phys. Rev. B **45**, 13244 (1992).
[23] T. A. Halgren and W. N. Lipscomb, Chem. Phys. Lett. **49**, 225 (1977).
[24] C. Rhodes, G. J. Hutchings, and A. W. Ward, Catal. Today **23**, 43 (1995), and references therein.
[25] P. Liu and J. A. Rodriguez, J. Phys. Chem. B **110**, 19418 (2006).
[26] J. Ren and S. Meng, J. Am. Chem. Soc. **128**, 9282 (2006).
[27] J. Nakamura, J. M. Campbell, and C. T. Campbell, J. Chem. Soc., Faraday Trans. **86**, 2725 (1990).
[28] P. Liu, J. A. Rodriguez, H. Hou, and J. T. Muckerman, J. Chem. Phys. **118**, 7737 (2003).
[29] N. Lopez and J. K. Nørskov, J. Am. Chem. Soc. **124**, 11262 (2002).
[30] A. Maiti, J. A. Rodriguez, M. Law, P. Kung, J. R. McKinney, and P. Yang, Nano Lett. **3**, 1025 (2003).
[31] J. Greeley, J. K. Nørskov, and M. Mavrikakis, Annu. Rev. Phys. Chem. **53**, 319 (2002).